Scientific Research Publishing

Journal of Applied Mathematics and Physics, 2023, 11, 649-662
https://www.scirp.org/journal/jamp
ISSN Online: 2327-4379
ISSN Print: 2327-4352

Surface Quantum-Dimensional Photocarrier Recombination in *CdTe* Microcrystals

Alexander Viktorovich Sel'kin[1], Nosirjon Khaydarovich Yuldashev[2*]

[1]Ioffe Institute, Saint Petersburg, Russia
[2]Fergana Polytechnic Institute, Fergana, Uzbekistan
Email: alexander.selkin@mail.ioffe.ru, *uzferfizika@mail.ru

How to cite this paper: Sel'kin, A.V. and Yuldashev, N.K. (2023) Surface Quantum-Dimensional Photocarrier Recombination in *CdTe* Microcrystals. *Journal of Applied Mathematics and Physics*, **11**, 649-662.
https://doi.org/10.4236/jamp.2023.113042

Received: January 28, 2023
Accepted: March 10, 2023
Published: March 13, 2023

Abstract

The scope of the study is the spectra of low-temperature (T = 2K) photoluminescence of a *p-CdTe/n-CdS* film heterostructure comprising a monolayer of *CdTe* microcrystals, where a single microcrystalline particle is typically one micron in size. Focus is made on the dominant band of "super-hot" emission appearing in the spectral region located in energy above the fundamental absorption edge of a *CdTe* bulk crystal. A theoretical model has been developed that assumes the existence of a space-charge layer inside a microcrystal, which leads to the formation of a triangular potential well for an electron near the surface. The anomalous emission band arises as a result of the optical transitions of electrons from near-surface levels of spatial quantization to valence band states.

Keywords

Photoluminescence, *CdTe* Microcrystals, *p-CdTe/n-CdS* Film Heterostructure, Quantum-Dimensional Effect, Exciton-Polariton

1. Introduction

Optical spectroscopy based on the study of low-temperature photoluminescence (*PL*) is an effective and non-destructive method for studying and monitoring the electronic, optical, and photoelectric characteristics of polycrystalline semiconductor film structures with photovoltaic properties [1] [2] [3]. Recently, *PL* data have been successfully used for the detailed characterization of *p-CdTe/n-CdS* film heterojunctions in solar cells (where the main absorbing layer is *p-CdTe* polycrystalline film), which is directly related to the topical issues of increasing the efficiency of such cells and improving their manufacturing technology [4] [5] [6] [7] [8]. In the works mentioned, the thickness h of the *CdTe* film and the av-

erage sizes d_{cr} of polycrystalline grains, as a rule, significantly exceeded the wavelength λ of the light in the spectral range of emission that was detected.

At the same time, the idea of the feasibility of producing solar cells from *p-CdTe*/*n-CdS* thin-film heterostructures with typical h and d_{cr} values of the order of λ have recently become a matter of discussions [8] [9] [10]. In such a case, a thin fine-grained *CdTe* film may have specific properties due to the presence of microcrystals. The issues of forming *PL* from such films have scarcely been considered before. However, it should be noted in this regard that the *PL* spectra of *CdS* microcrystals grown in the bulk of a transparent silicate glass matrix were studied in [11]. It was found that the *PL* spectra of rather large microcrystals (~70 nm) are similar to those of bulk crystals and are identified by known emission mechanisms (caused by the recombination of free and bound excitons, impurities, and lattice defects).

The work [12] studied the features of the *PL* spectra of thin pure and indium-doped *CdTe* polycrystalline films ($h \approx 0.5$ - $0.8\,\mu m$, $T = 2$ K) obtained by thermal vacuum evaporation on a glass substrate, depending on the content of point and structural defects. It has been shown that, in contrast to single crystals [13], large-block polycrystals [14] [15], and microcrystals [11], the *PL* spectra of fine-grain ($d_{cr} \sim 1\,\mu m$) films do not exhibit exciton and donor-acceptor pair emission channels.

The aim of this work is to study new mechanisms responsible for the formation of near-edge *PL* spectra which appear in a *p-CdTe*/*n-CdS* film heterostructure containing a thin *CdTe* polycrystalline layer. We draw attention to the possibility for the manifestation of low-dimensional effects in microcrystals possessing linear sizes of about one micron, *i.e.*, significantly exceeding the typical value of exciton Bohr radius a_{ex}.

The main effect is to observe in the low-temperature *PL* spectra of *CdTe* microcrystals the dominant narrow "superhot" emission band belonging to the spectral region located in energy above the fundamental absorption edge of the semiconductor material.

2. Objects under Study and Experimental Data

A *p-CdTe*/*n-CdS* film heterostructure (shown schematically in **Figure 1**) with an upper, *CdTe*, active absorbing layer was produced by thermal vacuum evaporation on a transparent glass substrate within a single technological cycle [12].

The lower, *CdS*, photo-resistive layer with an area of 20×5 mm^2 and a thickness of 0.2 - 0.4 μm had electronic conductivity. Under the mercury lamp illumination ($I_{Hg} \approx 10^4$ lx), the resistance of the *CdS* layer fell by 2 - 3 orders of magnitude. According to the results of the electron microphotography of the transverse cleavage and the *CdS* layer surface, the latter had a block-like columnar structure without pores, and the sizes of crystal blocks along the substrate surface were 1 - 3 μm. The *CdTe* layer with a thickness of h~0.5 - 0.8 μm was grown at a deposition rate of 1.5 - 2.0 Å/s at a substrate temperature of T~523 -

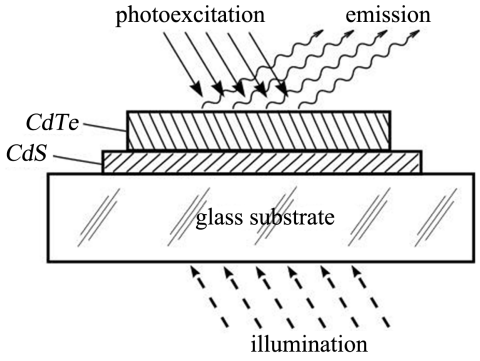

Figure 1. Schematic representation of the investigated *p-CdTe*/*n-CdS* film heterostructure grown on a glass substrate. Luminescence ("emission") was excited by Ar^+ laser light ("photoexcitation") with the possibility of turning on illumination ("illumination") in the *CdS* intrinsic absorption region.

623 K and had a granular structure with the size of cubic crystal grains d_{cr} ~ 0.8 - 1.0 μm. The active area of the *p-CdTe*/*n-CdS* heterostructure was 70 - 80 mm^2.

The scanning electron microscope picture of a surface fragment (f_4) and the transverse cleavage (f_3, f_2, f_1 layers) of the grown structure is shown in **Figure 2**. The f_4 and f_3 areas of the microphotogram represent the *CdTe* layer surface and transverse cleavage, respectively. The f_2 area belongs to the *CdS* layer deposited on the glass substrate (f_1).

To measure the *PL* spectra, the heterostructure was directly immersed in pumped liquid helium at a temperature of ~2 K. The spectra were recorded with a unit assembled on the basis of a DFS-24 spectrometer operating in the photon-counting mode. The frontal excitation of luminescence (from the open surface) of the *CdTe* layer was carried out at a wavelength of λ = 476.5 nm by Ar^+ laser light focused on the surface of the *CdTe* layer into a spot ~0.4 × 4 mm^2 in size at a luminous power of ~7 mW. The experiment was carried out in the geometry of normal (along the normal to the surface) photoexcitation and almost normal emission output.

Figure 3(a) shows the *PL* spectrum under the frontal excitation of the *CdTe* layer in the *p-CdTe*/*n-CdS* heterostructure. As can be seen from the figure, the spectrum of the structure contains an intense and dominant *A*-emission band (photon energy $\varepsilon_A = 1.6380$ eV, $\lambda_A = 757.0$ nm) located in energy much higher than the known [16] position $\varepsilon_g = 1.6065$ eV of the conduction-band edge in the *CdTe* crystal. A decrease in the intensity of light that excites *PL* from the outer side of the *CdTe* film is accompanied by a decrease in the emission intensity in the spectral range under study but it does not lead to a noticeable change in the shape of the spectrum.

However, it turned out that an essential change occurs in the general appearance of the *PL* spectrum (**Figure 3(b)**) when the heterostructure is additionally illuminated through transparent glass substrate (see **Figure 1**) using the light of a mercury lamp from the spectral region of *CdS* intrinsic absorption. The intensity of the *A*-band sharply decreases simultaneously with its spectral narrowing,

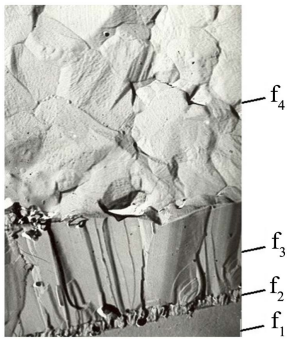

Figure 2. Microphotograph of the surface (f4) and transverse cleavage (layers f3, f2, f1) of the studied *p-CdTe/n-CdS* film heterostructure: f1—glass substrate, f2—*CdS* layer, f3—*CdTe* layer.

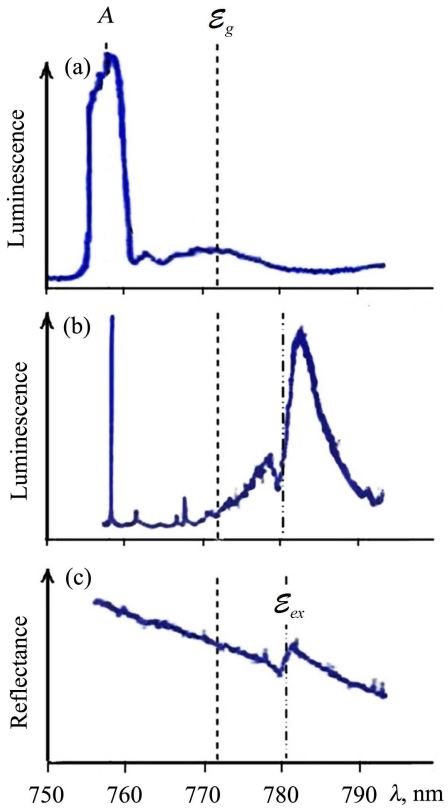

Figure 3. Photoluminescence spectra of the *p-CdTe/n-CdS* (T = 2K) hetero-structure upon the frontal excitation of the *CdTe* layer by Ar+ laser at the wavelength of λ = 476.5 nm ((a)—without additional illumination, (b)—with simultaneous illumination from the side of a substrate by the light of a mercury lamp within the spectral region of *CdS* intrinsic absorption). (c) Specular light reflection spectrum for the same structure from the *CdTe* layer side.

and a doublet emission band appears within the region of ~775 - 790 nm in the long-wavelength part of the spectrum, where $\varepsilon < \varepsilon_g$. As can be seen from the comparison with the specular reflection spectrum (**Figure 3(c)**), the minimum between the maxima of the doublet emission band is formed in the wavelength region, where the contour of reflection coefficient shows sharp dispersion de-

pendence.

3. Discussion of Results, Theory

In order to find out the cause of the observed "superhot" emission (**Figure 3(a)**) it should be noted that the structure studied actually includes a monolayer of closely spaced particles in the form of *CdTe* microcrystals, and each of these microcrystals has a typical linear size of ~1 μm. Therefore, we can talk about some dimensional effect due to the emission of light by each particle. However, given the relatively large average diameter of microcrystals that make up the structure, the possible dimensional effect is not similar to what is typical for quasi-zero-dimensional structures (quantum dots) [17] [18] [19].

At the same time, it is well known [20] that specific quantum effects can appear under certain conditions in the electrical properties of planar semiconductor systems when surface channels arise due to quantizing the energy of charge carriers in them. The main reason for the occurrence of such channels is the existence of a space-charge region (SCR). Due to the uncompensated space and surface charges of impurities, the bands (both conduction and valence bands) forming a near-surface potential well for sign-specific charge carriers are bent within this region. In this regard, it is of interest to analyze the possible light emission mechanism responsible for the spectrum formation (**Figure 3(a)**) and taking into account the features of carrier energy quantization in a near-surface quantum well.

1) Theoretical model

Let us turn to the simplified model of a microcrystal particle contained in a monolayer of the structure studied. We will consider this particle as a microcrystalline sphere of radius R (see **Figure 4**). The diameter $2R$ of the sphere is comparable to the typical average linear size of microcrystalline particles forming a monolayer. Since we are talking about *CdTe p*-type semiconductor material, it may be assumed the sphere contains a negatively charged SCR ($r_0 \le r \le R$) with the charge density ρ_q that is governed by the average excess concentration $N_A - N_D$ of the acceptor impurity against the donor one

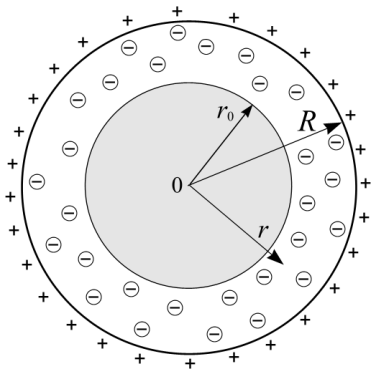

Figure 4. Spherical model of a *p-CdTe* microcrystalline particle. The states on the surface (sphere of radius R) are occupied by positively charged holes. The $r_0 \le r \le R$ layer is negatively charged. The central spherical region, $0 \le r < r_0$, is electrically neutral.

$$\rho_q = -e\left(N_A - N_D\right), \tag{1}$$

where e is the absolute value of electron charge. The capture centers of positively charged holes are localized on the surface of the sphere, $r = R$, and the full charge of such centers compensates for the space-charge of the microcrystalline sphere. The central spherical region, $0 \le r \le r_0$, is electrically neutral (excess acceptors in this region are electrically neutral).

In the approximation of the Schottky barrier model and with an account of the spherical symmetry of the problem, it is easy to obtain expressions for energy bands (conduction band $\mathcal{E}_c$ and valence band $\mathcal{E}_v$) in the form of dependencies on the radius r:

$$\mathcal{E}_c(r) = \mathcal{E}_v(r) + \mathcal{E}_g = \frac{2\pi e\rho_q}{3\varepsilon_{st}} r^2 \left(1 - 3\frac{r_0^2}{r^2} + 2\frac{r_0^3}{r^3}\right), \quad r_0 \le r \le R, \tag{2}$$

where $\mathcal{E}_g$ is the width of the bandgap, and ε_{st} is the static permittivity of a semiconductor. Expression (2) implies the normalization of electrostatic potential $\varphi(r) = -\mathcal{E}_c(r)/e$ so that $\mathcal{E}_c(r) = 0$ in the $0 \le r \le r_0$ range. This expression shows that the bands are bent downwards in energy within the microcrystalline sphere from its center to its surface, *i.e.*, an electron near-surface potential well of the depth $\left|\mathcal{E}_c(R)\right|$ is formed.

The built-in electric field strength $E(r)$ corresponding to dependence (2) in the microsphere is presented as follows:

$$E(r) = \frac{1}{e}\frac{\mathrm{d}\mathcal{E}_c}{\mathrm{d}r} = \frac{4\pi\rho_q}{3\varepsilon_{st}} r \cdot \left(1 - \frac{r_0^3}{r^3}\right), \tag{3}$$

where one should assume $E(r) = 0$ at $0 \le r \le r_0$. In accordance with the negative sign of ρ_q (see Equation (1)), the field strength vector is directed towards the center of the sphere.

The effects of dimensional quantization can appear just near the surface $r = R$ at the distances l_{QW} from the surface (see below) comparable to the de Broglie wavelength of an electron. Such effects were considered in sufficient detail earlier [20] when describing the phenomena of charge carrier transfer near the flat surfaces of semiconductors. The most significant results were obtained on the basis of modeling the surface potential in the form of a triangular potential well.

When analyzing our experimental data, we can use basic relations following from the known [20] [21] calculations for a one-dimensional triangular potential well if $l_{QW} \ll R$. The latter inequality shall be fulfilled well enough for the lowest energy states of a triangular quantum well, taking into account that the value R in the structures we studied is $R \approx 500$ nm.

According to [20], the $\mathcal{E}_n^{QW}$ energy of the quantum state n is found with a sufficiently high accuracy according to the following formula:

$$\mathcal{E}_n^{QW} = \left[\frac{3\pi\hbar e E_s}{2\sqrt{2m_*}}\left(n + \frac{3}{4}\right)\right]^{2/3}, \quad n = 0, 1, 2, \cdots, \tag{4}$$

where E_s is the electric field strength just on the surface, m_* is the effective mass of the charge carrier. Within the framework of the model discussed $E_s = |E(R)|$ (see Equation (3)). In the context of the lowest energy state $\mathcal{E}_0^{QW}$ Formulas (2) to (4) imply that

$$|\rho_q| = \frac{1}{3\pi^2}\frac{e\varepsilon_{st}\sqrt{m_*/m_0}}{Ra_B^2\left(1-r_0^3/R^3\right)}\left(\frac{\mathcal{E}_0^{QW}}{G_{Ry}}\right)^{3/2}, \tag{5}$$

where m_0 is the free-electron mass, a_B is the Bohr radius, and G_{Ry} is the Rydberg binding energy of an electron in a hydrogen atom.

Approximation $\mathcal{E}_c(r)$ by a triangular potential well $V(r)$ implies the equalities $\mathcal{E}_c = V$ and $d\mathcal{E}_c/dr = dV/dr$ at $r = R$, which gives

$$V(r) = \mathcal{E}_c(R) + (R-r)\cdot\frac{4e^2}{9\pi a_B^2}\cdot\sqrt{\frac{m_*}{m_0}}\left(\frac{\mathcal{E}_0^{QW}}{G_{Ry}}\right)^{3/2}. \tag{6}$$

Near the surface of the microsphere, the function $\mathcal{E}_c(r)$ is close to linear one and can be approximated by the triangular potential (6). The valence band $\mathcal{E}_v(r)$ is shifted downward by the energy $\mathcal{E}_g$ relative to $\mathcal{E}_c(r)$. In accordance with expression (4), the triangular well contains the lowest, $n = 0$, energy level of dimensional quantization that is shifted upward relative to the bottom of the well by the energy $\mathcal{E}_0^{QW}$. Under the external photo-excitation of carriers and as they relax in energy and momentum with the excitation of lattice vibrations, the electronic state $\mathcal{E}_0^{QW}$ is populated. The subsequent emission transition of an electron to the valence band is carried out with the creation of a photon with the energy $\hbar\omega = \mathcal{E}_A$. In this case, the transition probability maximum corresponds to the radius $r = r_{em}$ in the space, where the modulus of the wave function $\Psi(r)$ of an electron in the $n = 0$ state takes the maximum value. In the case of an infinitely high potential barrier on the sphere surface, the wave function shall contain a node located just on the surface $r = R$. Thus, maximum luminescence intensity shall be observed at the energy $\mathcal{E}_A$ (see Figure 5 showing the scheme of optical transition creating the peak A of emission).

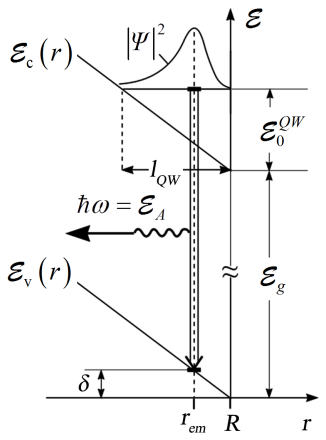

Figure 5. The scheme of the optical transition forming the peak of emission A with the energy $\mathcal{E}_A$ of a photon emitted.

$$\varepsilon_A = \varepsilon_g + \varepsilon_0^{QW} - \delta, \tag{7}$$

where the additional shift δ is determined by the r_{em} value.

The value of r_{em} can be estimated using a specific behavior of the wave function $\Psi(r)$ for the $n=0$ state. The exact solution of the Schrödinger equation for an ideal triangular well with walls of infinite height (one is vertical, the other is inclined) is expressed [20] in terms of the Airy functions. To estimate the position of the maximum of the function $|\Psi(z)|$ describing the $n=0$ state, we focus on the variational form of Ψ obtained in one-dimensional case (the axis z is directed perpendicular to the flat surface $z=0$ deep into the crystal) [21]:

$$\Psi(z) = \left(3b^3/2\right)^{1/2} z \cdot \exp\left[-(bz)^{3/2}/2\right], \tag{8}$$

where the parameter b is given by

$$b = 48\pi m_* e^2 \left(N_A - N_D\right) z_d / \varepsilon_{st} \hbar^2, \tag{9}$$

and contains the thickness of a depletion layer z_d which is found from the total energy minimum condition.

This representation has been successfully used in a number of studies when analyzing the phenomena of charge carrier transfer in the near-surface region of a semiconductor [20] [21].

It is easy to show that the maximum of function (8) is located at the point

$$z = z_{\max} = 2\sqrt[3]{6}/3b. \tag{10}$$

For the model we use (**Figure 4**) in formulae (8) to (10), we should make obvious substitutions as follows:

$z = R - r$, $z_d = R - r_0$, and $z_{\max} = R - r_{em}$.

Then

$$R - r_{em} = a_B \left(\pi/3\right)^{1/3} \sqrt{\frac{m_0}{m_*} \frac{G_{Ry}}{\varepsilon_0^{QW}}}. \tag{11}$$

On the other hand, as can be seen from **Figure 5**,

$$\frac{\delta}{R - r_{em}} = \frac{\varepsilon_0^{QW}}{l_{QW}}, \tag{12}$$

where l_{QW} is the width of the model triangular potential at the energy level ε_0^{QW}.

As it follows from Equation (6),

$$l_{QW} = a_B \cdot \frac{9\pi}{8} \sqrt{\frac{m_0}{m_*}} \cdot \sqrt{\frac{G_{Ry}}{\varepsilon_0^{QW}}}. \tag{13}$$

As a result, based on Equations (11) to (13) we have

$$\delta = \gamma \cdot \varepsilon_0^{QW}, \tag{14}$$

where the coefficient γ has a numerical value

$$\gamma = \frac{8}{9}\left(\frac{1}{3\pi^2}\right)^{1/3} \approx 0.287. \tag{15}$$

Thus, taking into account Equations (7) and (14), we can find the ε_0^{QW} value

$$\varepsilon_0^{QW} = \frac{\varepsilon_A - \varepsilon_g}{1-\gamma} \tag{16}$$

expressed through the experimental data concerning the energies ε_A and ε_g.

For the structure studied one obtains $\varepsilon_0^{QW} = 44.18$ meV and $\delta = 12.68$ meV.

The electric filed strength E_s on the surface is given by the expression

$$E_s = \left|E(R)\right| = \frac{e}{a_b^2} \cdot \frac{4}{9\pi} \cdot \sqrt{\frac{m_*}{m_0}} \cdot \left(\frac{\varepsilon_0^{QW}}{G_{Ry}}\right)^{3/2} \tag{17}$$

following from Equations (3) and (4). Assuming $m_*/m_0 = 0.11$ [22], we get $E_s = 44.6$ kV/cm.

For the width of the quantum well at the energy ε_0^{QW} (see Equation (13)) one obtains $l_{QW} = 9.9$ nm.

So, $l_{QW}/R \approx 0.02 \ll 1$, which corresponds to the initial assumptions for the model used in the estimates.

In addition, within the framework of the spherical model used, we can obtain the expression for the surface concentration N_s of charges at the microcrystal boundary

$$N_s = \frac{\varepsilon_{st}\sqrt{m_*/m_0}}{\left(3\pi a_B\right)^2}\left(\frac{\varepsilon_0^{QW}}{G_{Ry}}\right)^{3/2} \tag{18}$$

which at $\varepsilon_{st} = 10.6$ [23] gives $N_s = 2.6\times10^{11}$ cm^{-2}.

Thus, using the spectral position of the observed line A within the approximation of a triangular near-surface potential well, we found the values of the principal parameters ε_0^{QW}, E_s, l_{QW}, and N_s characterizing this well. Note that, when finding the numerical values of these parameters, the electro-neutrality radius r_0 ($0 \le r_0 < R - l_{QW}$) did not appear. However, as seen from Formulaes (1), (2), and (5), the parameter r_0 is directly associated with the band bending $\varepsilon_c(R)$ and the excess concentration $N_A - N_D$ of acceptors. In particular, at $r_0 = 0$ (the condition for the absence of an electrically neutral region), we have the minimum possible concentration of $\left|N_A - N_D\right|_{r_0=0} = 1.6\times10^{16}$ cm^{-3}, and the maximum possible band bending $\left|\varepsilon_c(R)\right|_{r_0=0} = 1.1$ eV.

Figure 3(a) shows that the emission line A is broadened and its half-width is $\Delta\varepsilon_A \approx 1.3$ meV, which is most likely due to inhomogeneous broadening processes. Indeed, in a more rigorous approach, one should consider the luminescence to arise actually from different locally planar near-surface elements with quantization energies ε_0^{QW} differing in value. The size of each element in the direction along the surface has to be of the order of the electron mean free path.

2) PL spectra of a microcrystalline *CdTe* layer under additional illumination

A very interesting and important effect from the point of view of possible practical applications is associated with the noticeable sensitivity of the PL spec-

trum to additional illumination of the structure from the transparent substrate side that we found (see **Figure 1** and **Figure 3(b)**). On the one hand, this illumination results in the actual disappearance of the "hot" luminescence band A $\left(\varepsilon_A > \varepsilon_g\right)$. On the other hand, the spectral region $\varepsilon < \varepsilon_g$ exhibits appearance of a doublet luminescence band, where the lowest exciton state with the energy of $\varepsilon_{ex} \approx 1.5955$ eV is recorded in fairly perfect bulk *CdTe* crystals) [24].

The direct relation of the PL band appearing in the spectral range of ~775 ÷ 790 nm under additional illumination to free excitons is confirmed by comparing the PL spectrum (**Figure 3(b)**) with the specular light reflection spectrum (**Figure 3(c)**) from the open surface of *CdTe* films. As can be seen from **Figure 3(b)** and **Figure 3(c)**, the dip in the doublet emission band is located in the wavelength region, where the reflection coefficient contour shows a typical resonant behavior. The doublet shape of the PL spectrum and its location relative to the light reflection contour indicate that we are dealing with the luminescence of exciton polaritons [25] [26].

The illumination-induced polariton luminescence can be explained as follows. Under illumination of the *n-CdS* layer with light of photon energy $\hbar\omega > \varepsilon_{g(CdS)}$, where $\varepsilon_{g(CdS)}$ is the width of the forbidden gap in *CdS*, the layer's intrinsic photoconductivity increases and the resistance of *n-CdS* turns out to be less than the resistance of the photovoltaic *p-CdTe* layer. Additional photogenerated electrons and holes compensate, respectively, for the surface positive charge of a microcrystal and the negative bulk charge of excess acceptors. As a result, the band bending within SCR decreases, which should lead to the disappearance of a near-surface potential well localizing an electron, and, as a consequence, to the disappearance of the *A* line.

On the other hand, with decreasing the band bending, the built-in electric field *E* determining the exciton lifetime decreases as well [27] [28]. This field becomes very weak under additional illumination, thus, allowing the exciton state to exist during a relatively long lifetime. As a sequence, the PL band associated with the emission of exciton polaritons appears in the region near ε_{ex}.

At sufficiently high E (of the order of 10^4 ÷ 10^5 V/cm) the exciton state is completely ionized. These are just the fields that act on the exciton in the *CdTe* layer when illumination is off. Therefore, PL band is not observed in the ε_{ex} region without illumination. In this case, the built-in electric field that destroys the exciton must occupy a sufficiently large volume, which corresponds to the limitation $\left(r_0/R\right)^3 \ll 1$ for the maximum value of r_0. The last inequality works well if we assume that $\left(r_0/R\right) < 0.5$. Then, for the microcrystals included in the structure we studied, the possible concentration of the excess acceptors and the total band bending should be within (1.6 to 1.8) × 10^{16} cm^{-3} and 0.64 to 1.1 eV, respectively.

In connection with the discussion of the illumination effect, it should be noted that the actual conditions under which such an effect manifests itself do not correspond accurately enough to the simplest spherical model of a microcrystal considered above. The spherical model makes it possible to identify, first of all,

the fundamental cause of the phenomenon, namely, the existence of quantizing levels for electrons in a thin surface layer of the sample. The effect of illumination becomes significant due to the presence of a thin *n-CdS* layer in the structure, which, in contact with *p-CdTe* microcrystals, forms in average flat heterointerface between two semiconductor materials. Additional photocarriers excited due to illumination are created in those regions of *CdTe* microcrystalline particles that are in direct contact with the *CdS* film. In this case, one should keep in mind, mainly, photo induced changes in the band bends related to the indicated regions of the particles.

4. Conclusions

The dimensional quantization effects inherent in various low-dimensional solid-state structures remain the subject of special interest from both scientific and practical perspective. When it comes to small crystals made of semiconductor materials, then, as a rule, the phenomena associated with microcrystal sizes comparable to the exciton Bohr radius a_{ex} are discussed.

This work presents the results of studying the quantum-size recombination of photocarriers in *CdTe* microcrystalline particles that have a linear size (one micron) significantly exceeding the typical value of a_{ex}. The main observed effect is the formation of the dominant narrow "superhot" emission band located in energy above the fundamental absorption edge of the bulk *CdTe* crystal. This "superhot" emission band is manifested in the low-temperature photoluminescence spectrum of the *p-CdTe/n-CdS* film heterostructure containing such particles. To understand the nature of the observed anomalous emission, a model of a spherical microcrystal is considered. According to this model, the sphere contains a near-surface space charge region, where the band bending occurs (both for conduction and valence bands) as it approaches the surface. In this case, a potential (triangular in shape) quantum well $V(r)$ for electrons is formed just near the surface. Hot emission band arises due to optical transitions of electrons from the quantized energy levels in the well to the quasi-continuous states of the valence band. Additional illumination of the heterostructure from the side of a transparent substrate with light within the spectral region of intrinsic absorption in *CdS* leads to quenching the anomalous short-wavelength emission band and simultaneously induces the *CdTe* exciton-polariton luminescence. This effect has a natural explanation if we take into account the illumination-associated generation of additional charge carriers that compensate for the positive charge of the microcrystal surface and the negative space charge of acceptors. In this case, the band bending is smoothed out, the near-surface potential well disappears, and the built-in electric field (which is so strong without illumination that the exciton-polariton state is not detected due to total exciton ionization) is weakened. From the standpoint of application, further studies of the luminescence spectra of *p-CdTe*/*n-CdS* film heterostructures with transparent ohmic contacts are of interest in order to develop new kind of solar cells based on them. Such studies should include a more thorough analysis of dependences on the micro-

crystal size, the CdS and *CdTe* thickness layers, the doping method, temperature, as well as the spectral composition and illumination intensity. The *p-CdTe*/*n-CdS* heterostructure studied is promising not only in terms of its practical application as an efficient photoconverter, but also for the development of methods for studying photoelectric phenomena in semiconductor micro- and nanostructures.

Conflicts of Interest

The authors declare no conflicts of interest regarding the publication of this paper.

References

[1] Tuteja, M., Koirala, P., Soares, J., Collins, R. and Rockett, A. (2016) Low Temperature Photoluminescence Spectroscopy Studies on Sputter Deposited CdS/CdTe Junctions and Solar Cells. *Journal of Materials Research*, **31**, 186-194. https://doi.org/10.1557/jmr.2015.399

[2] Durose, K., Asher, S.E., Gaegermann, W., Levi, D., *et al.* (2004) Physical Characterization of Thin-Film Solar Cells. *Progress in Photovoltaics Research and Applications*, **12**, 177-217. https://doi.org/10.1002/pip.542

[3] Caraman, I., Vatavu, S., Rusu, G. and Gasin, P. (2006) The Luminescence of CdS and CdTe Thin Films, Components of Photovoltaic Cells. *Chalcogenide Letters*, **3**, 1-7. https://chalcogen.ro/Caraman.pdf

[4] Ikhmayies, S.J. and Ahmad-Bitar, R.N. (2012) Interface Photoluminescence of the SnO_2:F/CdS:In/CdTe Thin Film Solar Cells Prepared Partially by the Spray Pyrolysis Technique. *Journal of Luminescence*, **132**, 502-506.

[5] Okamoto, T., Matsuzaki, Y., Amin, N., *et al.* (1998) Characterization of Highly Efficient CdTe Thin Film Solar Cells by Low-Temperature Photoluminescence. *Japanese Journal of Applied Physics*, **37**, 3894-3899. http://iopscience.iop.org/article/10.1143/JJAP.37.3894/meta

[6] Nakamura, K., Gotoh, M., Fujihara, T., Toyama, T., *et al.* (2001) Electromodulated Photoluminescence Study of CdS/CdTe Thin-Film Solar Cell. *Japanese Journal of Applied Physics*, **40**, 4508-4511. https://iopscience.iop.org/article/10.1143/JJAP.40.4508/meta

[7] Potter, M.D., Halliday, D.P., Cousins, M. and Durose, K. (2000) A Study of the Effects of Varying Cadmium Chloride Treatment on the Luminescent Properties of CdTe/CdS Thin Film Solar Cells. *Thin Solid Films*, **361-362**, 248-252. https://doi.org/10.1016/S0040-6090(99)00782-8

[8] Kosyachenko, L.A., Savchuk, A.I. and Grushko, E.V. (2009) Dependence of the Efficiency of a CdS/CdTe Solar Cell on the Absorbing Layer's Thickness. *Semiconductors*, **43**, 1023-1027. https://www.researchgate.net/publication/226518287

[9] Il'chuk, G.A., Kusnezh, V.V., Rud', V.Yu., Rud', Yu.V., Shapoval, P.Y. and Petrus', R.Yu. (2010) Photosensitivity of *n*-CdS/*p*-CdTe Heterotransitions Obtained by Chemical Surface Deposition of CdS. *Semiconductors*, **44**, 318-320. https://doi.org/10.1134/S1063782610030085

[10] Tuteja, M. (2014) Low Temperature Photo Luminescence Studies on Sputter Deposited Cadmium Sulphide/Cadmium Telluride Heterojunctions and Solar Cells. Thesis, University of Illinois at Urbana-Champaing, Urbana. https://hdl.handle.net/2142/50593

[11] Ekimov, A.I., Kudryavtsev, I.A., Ivanov, M.G. and Efros, A.L. (1990) Spectra and Decay Kinetics of Radiative Recombination in CdS Microcrystals. *Journal of Luminescence*, **46**, 83-95.

[12] Akhmadaliev, B.J., Mamatov, O.M., Polvonov, B.Z. and Yuldashev, N.K. (2016) Correlation between the Low-Temperature Photoluminescence Spectra and Photovoltaic Properties of Thin Polycrystalline CdTe Films. *Journal of Applied Mathematics and Physics*, **4**, 391-397.

[13] Akhmadaliev, B.Z., Polvonov, B.Z. and Yuldashev, N.K. (2014) Influence of Exciton Decay on the Polariton Luminescence Spectra of CdTe Crystal. *Optics and Spectroscopy*, **116**, 244-248. https://doi.org/10.1134/S0030400X14020027

[14] Ushakov, V.V., Klevkov, Yu.V. and Dravin, V.A. (2015) Ion implantation of Erbium into Polycrystalline Cadmium Telluride. *Semiconductors*, **49**, 630-633. https://link.springer.com/article/10.1134/S1063782615050267

[15] Bagaev, V.S., Klevkov, Yu.V., Kolosov, S.A., Krivobok, V.S. and Shepel', A.A. (2010) Optical and Electrophysical Properties of Defects in High-Purity CdTe. *Physics of the Solid State*, **52**, 37-42. https://link.springer.com/article/10.1134/S1063783410010075

[16] Fonthal, G., Tirado-Mejia, L., Marin-Hurta, J.I., Ariza-Calderón, H. and Mendoza-Alvarez, J.G. (2000) Temperature Dependence of the Band Gap Energy of Crystalline CdTe. *Journal of Physics and Chemistry of Solids*, **61**, 579-583. https://doi.org/10.1016/S0022-3697(99)00254-1

[17] Ekimov, A.I. and Onishchenko, A.A. (1981) Quantum Size Effect in Three-Dimensional Microscopic Semiconductor Crystals. *JETPLetters*, **34**, 345-349. https://www.researchgate.net/publication/234289541

[18] Ekimov, A.I., Kudryavtsev, I.A., Ivanov, M.G. and Efros, A.L. (1989) Photoluminescence of Quasi-Zero-Dimensional Semiconductor Structures. *Physics of the Solid State*, **31**, 192-207. http://mi.mathnet.ru/ftt5557

[19] Nozik, A.J., Beard, M.C., Luther, J.M., Law, M., Ellingson, R.J. and Johnson, J.C. (2010) Semiconductor Quantum Dots and Quantum Dot Arrays and Applications of Multiple Exciton Generation to Third-Generation Photovoltaic Solar Cells, *Chemical Reviews*, **110**, 6873-6890. https://doi.org/10.1016/S0022-3697(99)00254-1

[20] Ando, T., Fowler, A. and Stern, F. (1982) Electronic Properties of Two-Dimensional Systems. *Reviews of Modern Physics*, **54**, 437-672. https://doi.org/10.1103/RevModPhys.54.437

[21] Takada, Y. and Uemura, Y. (1977) Subband Structures of N-Channel Inversion Layers on III-V Compounds—A Possibility of the Gate Controlled Gann Effect. *Journal of the Physical Society of Japan*, **43**, 139-150. https://doi.org/10.1143/JPSJ.43.139

[22] Rubio-Ponce, A., Olguín, D. and Hernández-Calderón, I. (2003) Calculation of the Effective Masses of II-VI Semiconductor Compounds. *Superficies y Vacío*, **16**, 26-28. https://www.researchgate.net/publication/286929336

[23] Capper, P. and Garland, J., Eds. (2011) Mercury Cadmium Telluride: Growth, Properties and Applications. John Wiley & Sons, Inc., Hoboken. https://doi.org/10.1002/9780470669464

[24] Horodyský, P. and Hlídek, P. (2006) Free-Exciton Absorption in Bulk CdTe: Temperature Dependence. *Physica Status Solidi B*, **243**, 494-501. https://doi.org/10.1002/pssb.200541402

[25] Abukadyrov, A.G., Sazhin, M.I., Sel'kin, A.V. and Yuldashev, N.K. (1990) Polariton Luminescence of Mixed Modes in Crystals with Spatial Dispersion. *JEPT*: *Journal of*

Experimental and Theoretical Physics, **70**, 359-369.
http://www.jetp.ras.ru/cgi-bin/dn/e_070_02_0359pdf

[26] Sel'kin, A.V. and Yuldashev, N.Kh. (1992) Effects of Spatial Dispersion and Exciton Damping in Polariton Luminescence Spectra. In: Koptev, Yu.I., Ed., *Semiconductor and Insulators*: *Optical and Spectroscopic Research*, Ioffe Physico-Technical Institute Research Studies, Nova Science Publishers, Inc., Commack, 55-84.

[27] Novikov, A.B., Novikov, B.V., Yuferev, R.B., Roppischer, H., Stein, N. and Sel'kin, A.V. (1996) Anomalous Stark Effect on Excitonic States in a Preionization Electric Field. *Journal of Experimental and Theoretical Physics Letters*, **64**, 42-46. https://doi.org/10.1134/1.567156

[28] Romanovsky, S.O., Selkin, A.V., Stamov, I.G. and Feoktistov, N.A. (1998) Excitons in ZnP_2 Crystals in the Electric Field of a Schottky Barrier. *Physics of the Solid State*, **40**, 814-815. https://link.springer.com/article/10.1134/1.1130407